Soft Deployable Structures via Core-Shell Inflatables

Trevor J. Jones,[1] Thomas Dupuis,[1] Etienne Jambon-Puillet,[1] Joel Marthelot,[1,2] and P.-T. Brun[1,*]
[1]Department of Chemical and Biological Engineering, Princeton University, Princeton, New Jersey 08540, USA
[2]Aix-Marseille University, CNRS, IUSTI, 13013, Marseille, France

(Received 31 May 2022; accepted 3 February 2023; published 20 March 2023)

Deployable structures capable of significant geometric reconfigurations are ubiquitous in nature. While engineering contraptions typically comprise articulated rigid elements, soft structures that experience material growth for deployment mostly remain the handiwork of biology, e.g., when winged insects deploy their wings during metamorphosis. Here we perform experiments and develop formal models to rationalize the previously unexplored physics of soft deployable structures using core-shell inflatables. We first derive a Maxwell construction to model the expansion of a hyperelastic cylindrical core constrained by a rigid shell. Based on these results, we identify a strategy to obtain synchronized deployment in soft networks. We then show that a single actuated element behaves as an elastic beam with a pressure-dependent bending stiffness which allows us to model complex deployed networks and demonstrate the ability to reconfigure their final shape. Finally, we generalize our results to obtain three-dimensional elastic gridshells, demonstrating our approach's applicability to assemble complex structures using core-shell inflatables as building blocks. Our results leverage material and geometric nonlinearities to create a low-energy pathway to growth and reconfiguration for soft deployable structures.

DOI: 10.1103/PhysRevLett.130.128201

Decades of engineering research have led to the development of a broad range of deployable structures whose shapes vary from compact, folded configurations to expanded and operational configurations. Examples range from mundane umbrellas to ultralight spacecraft and antennas [1]. The field remains very active, with recent developments leveraging the newest insights from physics and mathematics, as well as the advanced computational power and manufacturing techniques available today to create mechanical metamaterials, architected structures, origami and kirigami systems [2–8]. Yet, most man-made deployable structures differ from those found in nature's long-evolving fauna, which not only use joints [9–11] but frequently comprise materials that grow, stretch, and bend to transform [12–14]. However, biology's simple strategy, which inherently uses lightweight and soft materials, is much more challenging to engineer. The rigid elements connected by a finite number of moving joints are replaced by continuously deformable soft materials undergoing large deformations in potentially all directions. In the thrust for biomimicry, there has been a push to develop, design, and manufacture shape-morphing matter that can robustly and predictably change shape (e.g., mechanical metamaterials [15], 4D printed materials [16–19], and soft robotics [20–22]). A key challenge and opportunity for these systems made of soft solids is the susceptibility to mechanical instabilities such as bulging, buckling, or wrinkling [23–27].

Here we take inspiration from the expansion of wings during metamorphosis [see Fig. 1(a)] in holometabolous insects to design soft structures whose expanded shapes can be programmed by the arrangement of vein structures. When insects (e.g., dragonflies, butterflies, cicadas) emerge, their wings are a compact, crumpled network of interconnected fluidic segments (veins) connected by a wrinkled membrane. Hemolymph, a bloodlike fluid, is injected into the wing [28,29], which first unfurls in a couple of minutes and then stiffens into its robust, flight-worthy, expanded form. The cross section of dragonfly wing veins shows a composite ultrastructure composed of a core-shell structure with an endocuticle rich in rubberlike protein (resilin [30]) surrounded by a rigid, thin exocuticle [31]. Motivated by this structure, we build a core-shell inflatable consisting of a soft hyperelastic rubber tube enclosed in inextensible sleeves whose length exceeds that of the tubes. We take advantage of the material nonlinearities of the hyperelastic elastomer which can undergo large deformation at constant pressure through a propagative instability [32–34]. While not detrimental to the inflation of a single tube, this instability hampers the smooth inflation of a network of hyperelastic tubes since when the instability occurs in one tube, all the injected gas in the network diverts to a single bulge (see movie S1). By limiting the core radial expansion, we alter the bulging instability to allow multiple elements to inflate at once (see movie S1). As detailed next, we show that a network of artificial veins connected by an inextensible and pleated membrane can be inflated to achieve a target shape [Fig. 1(b) and movie S2] and is a low-energy pathway strategy for growth and reconfiguration of soft deployable structures.

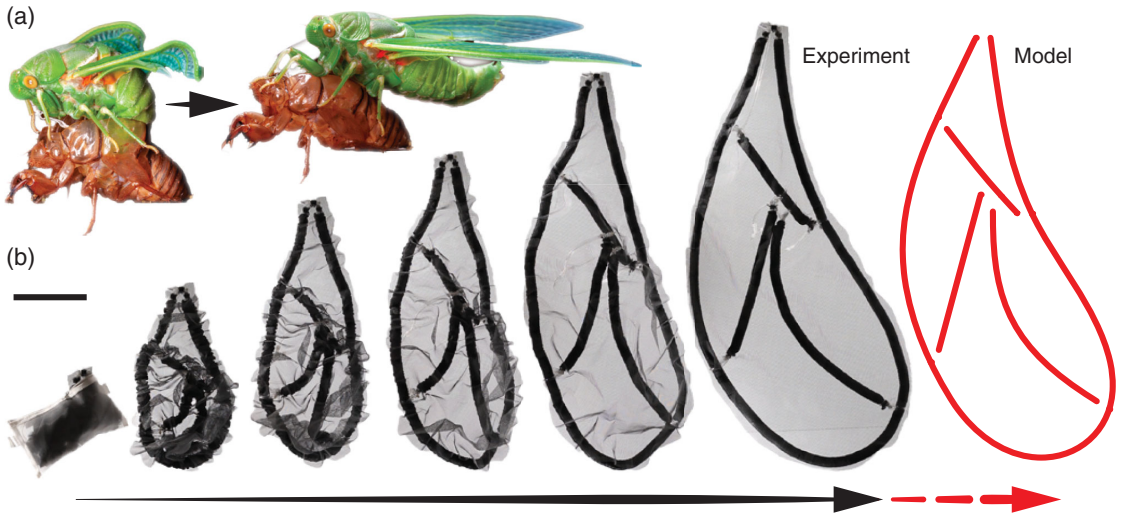

FIG. 1. Veinlike deployable structure. (a) Images of a cicada deploying its wings following molting its exoskeleton (Tacio Philip Sansonovski/Shutterstock.com). (b) Sequence of images showing a winglike structure that expands synchronously in a plane as pressure increases (scale bar, 15 cm). The prediction of the shape by elastic beams is drawn in red.

We first investigate how an inextensible shell impacts the bulging instability of hyperelastic balloons. In our core-shell system, a shell of radius R_s and shear modulus μ_s constrains a softer hyperelastic core of initial radius $R < R_s$ and modulus $\mu \ll \mu_s$. Figure 2(a) shows the pressure recorded during the inflation of a latex tube constrained by polytubing shells of various radii R_s and prewrinkling conditions. In all cases, we observe a monotonic increase in pressure up to a maximum P_m followed by a pressure drop and a quasiconstant plateaued propagating pressure P_p. In effect, our constructs undergo a bulging instability at P_m [see inset in Fig. 2(a) and movie S1], but the pressure drop after the instability $P_m - P_p$ appears to be reduced as R_s decreases. Experiments with straight, thick acrylic shells and finite element simulations with undeformable, straight, frictionless shells and a Gent hyperelastic core show very similar behavior [see Supplemental Material (SM) [35] section "FEM simulations for a constrained balloon" and the dashed lines in Fig. 2(a)].

To model the bulging instability of core-shell systems, we use the classical Maxwell construction (described in detail in SM [35] section "Maxwell construction"). The Maxwell construction for phase coexistence at a pressure P_p in cylindrical balloons requires the work done by the change in volume $(V_b - V_u)$ between the bulged volume V_b and quasi-unstretched volume V_u to equal the work done by the membrane stretching.

$$P_p(V_b - V_u) = \int_{V_u}^{V_b} P(V)dV. \tag{1}$$

Equation (1) has the geometric solution of equal areas between the isobar P_p and the membrane pressure-volume relationship $P(V)$ as illustrated in Fig. 2(b). In our system, the shell has the primary function of altering the pressure-volume relationship and thus the solution to Eq. (1).

We consider the shell to be inextensible, $PR_s/\mu_s h_s \ll 1$, and to freely wrinkle under compression, $PR_s^3/\mu h_s^3 \gg 1$ (see SM [35] section "Core-shell inflatable assumptions"). In practice, as the core is inflated to the shell radius, the shell maintains the excess stress as pressure keeps increasing. Therefore the shell provides a geometric constraint that prevents the radial expansion of the core above the shell radius R_s as pressure increases. As illustrated in Fig. 2(b), this geometric constraint causes the pressure $P(V)$ to diverge at the volume V_b^* where the core fills the shell. Applying Maxwell's construction, we find that core-shell structures have a higher propagating pressure P_p^* as the shell determines the maximum volume V_b^* of the core's bulged region during inflation.

In Fig. 2(c) we report the rescaled pressure drop $(P_m - P_p)/P_m$ plotted against the core-shell radius ratio R_s/R for experiments and simulations. All the data collapse on a master curve, confirming that the system is scale invariant and that both prewrinkling and the shell material have no measurable effect. The pressure drop decreases monotonically from the unconstrained value (for $R_s/R \gtrsim 5.8$ the bulged radius is less than the shell radius) to approximately zero for $R_s/R \approx 2$ (which is the core circumferential stretch at the onset of bulging). Our Maxwell construction implemented using a hyperelastic Gent model for the core (see SM [35] Section 1) compares favorably with experiments [see the line in Fig. 2(c)]. Note that in experiments, the plateau pressure is noisy when a shell is used [see the error bars in Fig. 2(c)]. For the most constrained systems ($R_s/R \simeq 2$) the pressure drop can even become negative, so that the system is at times above the critical bulging pressure P_m.

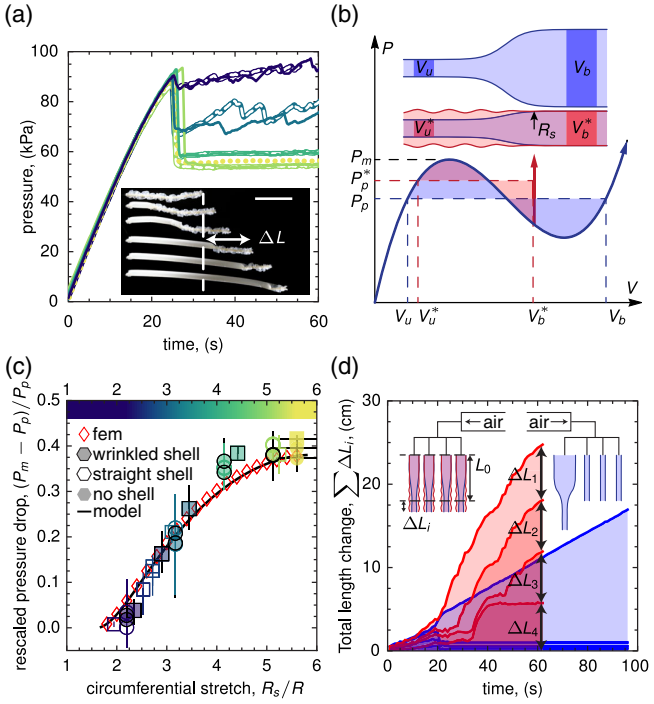

FIG. 2. Inflation of core-shell balloons. (a) Representative pressure curves of the tubes during inflation. The solid lines represent wrinkled shells, the dashed lines represent straight shells, and the dotted line is no shell. Color represents the core-shell radius ratio [see the color bar in (c)]. The inset shows typical images of core-shell inflation (scale bar, 30 cm). (b) Schematic for the Maxwell construction for the bulging of a cylindrical balloon and a core-shell balloon. (c) Plot of the pressure drop against the core-shell radius ratio. Markers represent experiments (circles: $R = 3.7$ mm, squares: $R = 7.3$ mm) and finite element simulations (diamonds). The line is the Maxwell construction model (see SM [35] Section 1). The error bars represent the range of the pressure measurements in the plateaued region following the bulging instability. (d) Plot of the accumulated length for a balloon system and core-shell system during inflation. Inset shows schematic of experiment.

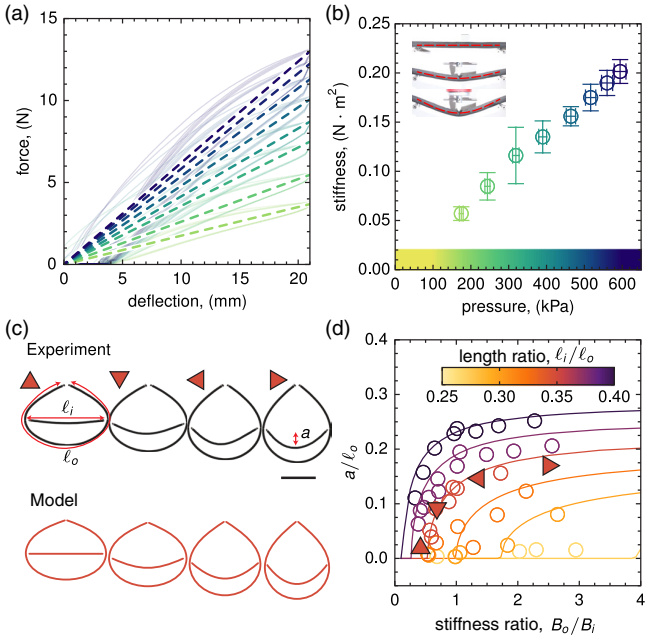

FIG. 3. Mechanics of inflated core-shell structures. (a) Force displacement curves of core-shell inflatables undergoing three point bending tests at different pressures. Color represents pressure [see color bar (b)]. (b) The effective bending stiffness B_{eq} plotted against the pressure difference P. Error bars show the local stiffness's standard deviation for the deflection range measured. (c) Images of an inflatable network where the pressures P of the inner and outer beams are controlled independently (scale bar, 30 cm) compared to our model. (d) Amplitude of the inner beam deflection from (c) plotted against the outer beam stiffness: inner beam stiffness ratio. Markers are experimental data [triangle markers represent images in (c)]. The lines are the predicted amplitudes from our model. Error bars are smaller than the markers.

We leverage this predictive knowledge to help smoothly expand an interconnected network of inflatables. To nucleate and propagate bulges in all of the inflatables concomitantly, we minimize the pressure drop $(P_m - P_p)$ using shells of radius $R_s \approx 2R$. In Fig. 2(d) we report the cumulative change in length of four of our interconnected inflatables [$R = 3.7$ mm, $L = 10$ cm and $R_s = 9.1$ mm, $L_s = 17.5$ cm], with (red) or without (blue) shells. As evident from the figure, we observe the nearly simultaneous expansion of all core-shell inflatables, while in the same system without the shell, only one core expands. We attribute this nearly simultaneous expansion to the significant fluctuations of the pressure plateau in our inflatables. These fluctuations allow the pressure in the system to exceed the critical pressure P_m, even after bulging has occurred, thereby enabling other bulges to nucleate.

Now that we understand how our core-shell system expands, we investigate the shape and mechanics of a deployed core-shell inflatable. Once inflated, the core-shell system becomes noticeably more rigid, for example, it is able to sustain its own weight. We perform three-point bending mechanical tests on a single inflatable to quantify this effect while varying the pressure. The force versus deflection curves are shown in Fig. 3(a) for a latex core and a prewrinkled polyester fabric shell for pressures ranging from $P_p \approx 100$ kPa to roughly $5P_p$. For a given pressure, the force initially increases linearly with the deflection before eventually softening akin to the bending of hollow tubes [36]. Within the experimental pressure range, the force required to bend the core-shell inflatable increases with the pressure. We extract an effective bending stiffness B_{eq} from the data to quantify this stiffening. This equivalent stiffness increases linearly with the pressure as reported in Fig. 3(b).

Knowing the rigidity of our core-shell structures, we leverage their slenderness ($L_s \gg R_s$) to model the nonlinear mechanics of our inflatables as Kirchhoff rods, i.e., a one-dimensional model for inextensible and unshearable elastic rods (see SM [35] Section 3). For a network, each

element thus has its own system of equations, with the key parameters being the deployed length, which is the length of the unwrinkled shell L_s, and the stiffness of the element B_{eq}. These equations are then coupled with the appropriate boundary and jump conditions at the connecting points, which depend on the type of connection and are derived on a case-by-case basis (see SM [35] section "Boundary and jump conditions"). We find a favorable agreement between the model and experiment, e.g., in the case of the winglike network of Fig. 1 and for the three-point bending experiments [Fig. 3(b) inset]. Furthermore, the fact that $B_{\mathrm{eq}} \propto P$ greatly broadens the range of accessible shapes since it is possible to control the stiffness of individual elements by connecting them to different pressure sources. We leverage this effect to dynamically reconfigure the network once deployed by varying the pressure inside a few key elements, all of which can be modeled by our reduced Kirchhoff model.

In Fig. 3(c) an outer element of length ℓ_o encloses an inner one of length ℓ_i attached to a separate pressure source (both beams are torque free at their ends). By manipulating the relative pressures of the two elements, we control the inner and outer rod bending stiffness B_i and B_o independently. As illustrated in Fig. 3(c), the inner rod buckles when we decrease its stiffness (comparatively to the outer one) by decreasing the pressure, which changes the global shape of this simple two-rod network from a wide to a narrow loop. To quantify this reconfiguration, we measure the buckling amplitude a of the inner beam and plot it in dimensionless form as a function of the stiffness ratio in Fig. 3(d) for a variety of rod length ratios ℓ_i/ℓ_o. As one could intuitively expect, the longer the inner element, the larger the shape change upon reconfiguration. As shown in Figs. 3(c) and 3(d), our reduced rod network model is fully capable of predicting these shape changes and thus can be used to design complex reconfigurable and deployable structures.

Because the core-shell network can be captured by elastic rods, we adapt the geometric approach developed for elastic gridshells [37] to design three-dimensional deployable structures. As an example, we build a flat network that deploys into a hemisphere [Fig. 4(a)]. Specifically, we create an elastic gridshell from a square lattice of core-shell inflatables with joints that can freely shear by using the geometry of Chebyshev nets [37]. Our square network is chosen so that each element's shell length L_s matches the target hemisphere section length. Last, we attach rigidly the boundary of our grid to the required flat contour. Figure 4(b) and movie S3 show the inflation of such a network using latex tubing in prewrinkled polyester fabric. The deployed form is well captured by the proposed Chebyshev net and is amenable to different geometries [37].

In closing, we note that our model is scale invariant. As such our theoretical framework and its ensuing conclusions are potentially relevant to biological systems, e.g., for the healthy deployment of insect wings during metamorphosis, and could be leveraged to design the future generation of robotic insects [38]. In effect, the inherently soft materials we used can undergo large deformations in both the deployed and undeployed states, thereby making these systems robust and suitable for miniaturization. Furthermore, we have demonstrated that our inflatables are reconfigurable via the modulation of their effective bending stiffness, which is achieved by controlling their internal pressure. Similar effects on controllable bending stiffness have been seen in pressurized hyperelastic tubes [39] and layered systems with internal friction [40] and have been theorized to play a role in cell stability [41]. Finally, we note that the inflation progression from undeployed to local bulges to fully deployed shows intermediate higher order modes [see Fig. 4(b) and movie S3], indicating the potential to build multistable networks with configurations that could be accessed via sequential deployment [8,19].

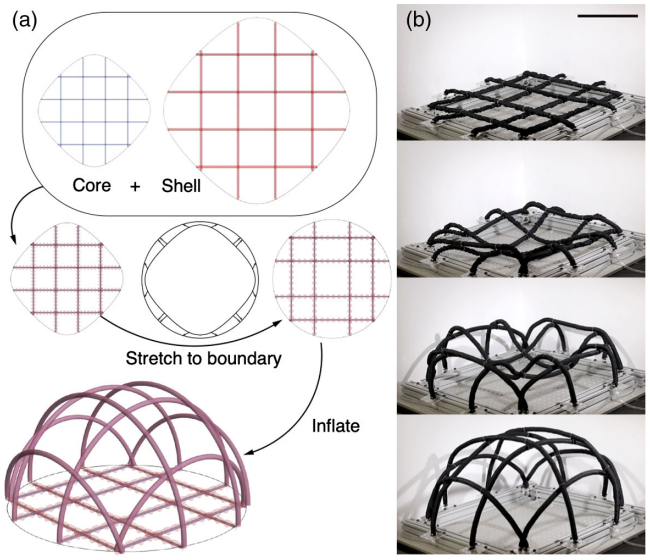

FIG. 4. Deployable elastic gridshells. (a) Design process for a deployable elastic gridshell from core-shell inflatables. (b) Inflation of a deployable elastic gridshell (scale bar, 25 cm).

E. J.-P. was partially supported by NSF through the Princeton University Materials Research Science and Engineering Center (Grant No. DMR-1420541), and T. J. J. and P.-T. B. were partially supported by NSF CAREER award (CBET 2042930) and NSF FMRG award (CMMI 2037097) T. J. J., E. J.-P., and P.-T. B. wrote the manuscript. J. M. and P.-T. B. conceived the project. T. J. J. and T. D. conducted the experiments. T. J. J., T. D., and P.-T. B. conceived the reduced models. E. J.-P. performed the finite element simulations.

*Corresponding author.
pierrethomas.brun@gmail.com

[1] Sergio Pellegrino, Deployable structures in engineering, in *Deployable Structures* (Springer, New York, 2001).

[2] Evgueni T. Filipov, Tomohiro Tachi, and Glaucio H. Paulino, Origami tubes assembled into stiff, yet reconfigurable structures and metamaterials, Proc. Natl. Acad. Sci. U.S.A. **112**, 12321 (2015).
[3] Wei Wang, Chenzhe Li, Hugo Rodrigue, Fengpei Yuan, Min-Woo Han, Maenghyo Cho, and Sung-Hoon Ahn, Kirigami/origami-based soft deployable reflector for optical beam steering, Adv. Funct. Mater. **27**, 1604214 (2017).
[4] Zirui Zhai, Yong Wang, and Hanqing Jiang, Origami-inspired, on-demand deployable and collapsible mechanical metamaterials with tunable stiffness, Proc. Natl. Acad. Sci. U.S.A. **115**, 2032 (2018).
[5] Daniela Rus and Michael T. Tolley, Design, fabrication and control of origami robots, Nat. Rev. Mater. **3**, 101 (2018).
[6] Stefano Mintchev, Jun Shintake, and Dario Floreano, Bio-inspired dual-stiffness origami, Sci. Rob. **3**, eaau0275 (2018).
[7] Julian Panetta, Mina Konaković-Luković, Florin Isvoranu, Etienne Bouleau, and Mark Pauly, X-shells: A new class of deployable beam structures, ACM Trans. Graph. **38**, 1 (2019).
[8] David Melancon, Benjamin Gorissen, Carlos J. García-Mora, Chuck Hoberman, and Katia Bertoldi, Multistable inflatable origami structures at the metre scale, Nature (London) **592**, 545 (2021).
[9] Lakshminarayanan Mahadevan and Sergio Rica, Self-organized origami, Science **307**, 1740 (2005).
[10] Kazuya Saito, Shuhei Nomura, Shuhei Yamamoto, Ryuma Niiyama, and Yoji Okabe, Investigation of hindwing folding in ladybird beetles by artificial elytron transplantation and microcomputed tomography, Proc. Natl. Acad. Sci. U.S.A. **114**, 5624 (2017).
[11] K. Saito, S. Yamamoto, M. Maruyama, and Y. Okabe, Asymmetric hindwing foldings in rove beetles, Proc. Natl. Acad. Sci. U.S.A. **111**, 16349 (2014).
[12] J. F. V. Vincent, Deployable structures in nature: Potential for biomimicking, Proc. Inst. Mech. Eng., Part C **214**, 1 (2000).
[13] Julien Dervaux and Martine Ben Amar, Morphogenesis of Growing Soft Tissues, Phys. Rev. Lett. **101**, 068101 (2008).
[14] Vincent Mirabet, Pradeep Das, Arezki Boudaoud, and Olivier Hamant, The role of mechanical forces in plant morphogenesis, Annu. Rev. Plant Biol. **62**, 365 (2011).
[15] C. Coulais, E. Teomy, K. de Reus, Y. Shokef, and M. van Hecke, Combinatorial design of textured mechanical metamaterials, Nature (London) **535**, 529 (2016).
[16] Yael Klein, Efi Efrati, and Eran Sharon, Shaping of elastic sheets by prescription of non-euclidean metrics, Science **315**, 1116 (2007).
[17] Jungwook Kim, James A. Hanna, Myunghwan Byun, Christian D. Santangelo, and Ryan C. Hayward, Designing responsive buckled surfaces by halftone gel lithography, Science **335**, 1201 (2012).
[18] A. Sydney Gladman, Elisabetta A. Matsumoto, Ralph G. Nuzzo, Lakshminarayanan Mahadevan, and Jennifer A. Lewis, Biomimetic 4d printing, Nat. Mater. **15**, 413 (2016).
[19] Ruslan Guseinov, Connor McMahan, Jesús Pérez, Chiara Daraio, and Bernd Bickel, Programming temporal morphing of self-actuated shells, Nat. Commun. **11**, 1 (2020).
[20] Emmanuel Siéfert, Etienne Reyssat, José Bico, and Benoît Roman, Bio-inspired pneumatic shape-morphing elastomers, Nat. Mater. **18**, 24 (2019).
[21] Elliot W. Hawkes, Laura H. Blumenschein, Joseph D. Greer, and Allison M. Okamura, A soft robot that navigates its environment through growth, Sci. Rob. **2**, eaan3028 (2017).
[22] Trevor J. Jones, Etienne Jambon-Puillet, Joel Marthelot, and P.-T. Brun, Bubble casting soft robotics, Nature (London) **599**, 229 (2021).
[23] Johannes T. B. Overvelde, Tamara Kloek, Jonas J. A. D'haen, and Katia Bertoldi, Amplifying the response of soft actuators by harnessing snap-through instabilities, Proc. Natl. Acad. Sci. U.S.A. **112**, 10863 (2015).
[24] Pedro M. Reis, A perspective on the revival of structural (in) stability with novel opportunities for function: from buckliphobia to buckliphilia, J. Appl. Mech. **82**, 111001 (2015).
[25] Katia Bertoldi, Vincenzo Vitelli, Johan Christensen, and Martin Van Hecke, Flexible mechanical metamaterials, Nat. Rev. Mater. **2**, 17066 (2017).
[26] Yinlong Tan, Biru Hu, Jia Song, Zengyong Chu, and Wenjian Wu, Bioinspired multiscale wrinkling patterns on curved substrates: An overview, Nano-Micro Lett. **12**, 1 (2020).
[27] Emmanuel Siéfert and Benoît Roman, Morphogenesis through elastic phase separation in a pneumatic surface, C. R. Méc. **348**, 649 (2020).
[28] Robert Moreau, Variations de la pression interne au cours de l'émergence et de l'expansion des ailes chez bombyx mori et pieris brassicae, J. Insect Physiol. **20**, 1475 (1974).
[29] Lutz Thilo Wasserthal, Interaction of circulation and tracheal ventilation in holometabolous insects, in *Advances in Insect Physiology* (Elsevier, New York, 1996), Vol. 26, pp. 297–351.
[30] Jan Michels, Esther Appel, and Stanislav N. Gorb, Resilin–the pliant protein, in *Extracellular Composite Matrices in Arthropods* (Springer, New York, 2016), pp. 89–136.
[31] Esther Appel, Lars Heepe, Chung-Ping Lin, and Stanislav N. Gorb, Ultrastructure of dragonfly wing veins: Composite structure of fibrous material supplemented by resilin, J. Anat. **227**, 561 (2015).
[32] E. Chater and John W. Hutchinson, On the propagation of bulges and buckles, J. Appl. Mech. **51**, 269 (1984).
[33] Stelios Kyriakides and Chang Yu-Chung, The initiation and propagation of a localized instability in an inflated elastic tube, Int. J. Solids Struct. **27**, 1085 (1991).
[34] Claire Lestringant and Basile Audoly, A diffuse interface model for the analysis of propagating bulges in cylindrical balloons, Proc. R. Soc. A **474**, 20180333 (2018).
[35] See Supplemental Material at http://link.aps.org/supplemental/10.1103/PhysRevLett.130.128201 for information about the materials and methods, and the legends of the supporting movies.
[36] L. G. Brazier, On the flexure of thin cylindrical shells and other "thin" sections, Proc. R. Soc. A **116**, 104 (1927).

[37] Changyeob Baek, Andrew O. Sageman-Furnas, Mohammad K. Jawed, and Pedro M. Reis, Form finding in elastic gridshells, Proc. Natl. Acad. Sci. U.S.A. **115**, 75 (2018).

[38] Noah T. Jafferis, E. Farrell Helbling, Michael Karpelson, and Robert J. Wood, Untethered flight of an insect-sized flapping-wing microscale aerial vehicle, Nature (London) **570**, 491 (2019).

[39] William J. Douglas, Bending stiffness of an inflated cylindrical cantilever beam, AIAA J. **7**, 1248 (1969).

[40] Samuel Poincloux, Tian Chen, Basile Audoly, and Pedro M. Reis, Bending Response of a Book with Internal Friction, Phys. Rev. Lett. **126**, 218004 (2021).

[41] Luyi Qiu, John W. Hutchinson, and Ariel Amir, Bending Instability of Rod-Shaped Bacteria, Phys. Rev. Lett. **128**, 058101 (2022).